J. Fluid Mech. (2009), *vol.* 641, *pp.* 463–473.
doi:10.1017/S0022112009991972

Noise radiation from a ducted rotor in a swirling-translating flow

ERIKA QUARANTA AND DIMITRIS DRIKAKIS†

Fluid Mechanics and Computational Science Group, Department of Aerospace Sciences, Cranfield University, Cranfield MK43 0AL, UK

(Received 18 June 2009; revised 3 September 2009; accepted 4 September 2009)

This paper investigates the noise radiation produced by a rotor inside a duct, which is convected by a swirling-translating mean flow. The study is based on an extension of Gennaretti's and Morino's boundary element method to the frequency domain for scattering problems in conjunction with a spinning rotor source model in the presence of a swirl flow. The proposed formulation is validated against exact solutions and is further used to investigate the effects of the translating flow Mach number and swirling flow angular velocity on noise radiation to the far field. The scattered sound is highly affected by the convecting mean flow. The modal content of the scattered field increases when increasing the translating flow Mach number, while a swirling flow leads to a reduction of the mode propagation, if co-rotating with respect to the azimuthal order of the spinning source, or an increase of the modal content, if counter-rotating with respect to the source. In general, the mean translating flow moves the main lobes of the directivity patterns downstream, while in some cases the mean swirling flow neglects this effect and the downstream lobe is completely shifted.

Key words: aeroacoustics, compressible flows

1. Introduction

One of the main sources of aircraft noise is the engine. There are several fluid dynamics phenomena involved in the sound generation. Turbulence is mainly responsible for the jet flow noise and the broadband component of turbomachinery noise. Unsteady aerodynamic loads on the compressor, fan and turbine rotor blades, interacting with stator blade rows, produce tonal noise, which propagates to the far field after being strongly modified by the intake and exhaust ducts.

This paper investigates the effects of the mean swirling-translating flow on the tonal noise generated by a single rotor in a duct. In contrast to the case of purely convected waves in a duct, in swirling flows the waves do not form a complete basis system for all wave types and they must, therefore, be constructed numerically (Tam & Auriault 1998; Gobulev & Atassi 2000; Heaton & Peake 2006). Generally, the presence of swirl can cut on or cut off modes depending on the sense of rotation with respect to the mean swirl. Modes cut on in the absence of mean swirl, but co-rotating with the swirl, are cut off by the swirl effect, whereas modes cut off in the absence of mean swirl, but counter-rotating with the swirl, are cut on by the swirl effect (Cooper & Peake 2005).

Several numerical methods has been employed to tackle the turbomachinery noise problem. More recently, computational aeroacoustics (CAA) methods have been most widely applied. CAA is a computational approach for solving the unsteady fluid flow

† Email address for correspondence: d.drikakis@cranfield.ac.uk

equations using computational fluid dynamics (CFD) methods, with special emphasis on resolving acoustic perturbations (Tam 2006). The CAA analysis accounts for the complexity of turbomachinery flow, however, because of the very fine scale necessary for the acoustic analysis, it is computationally very expensive to apply it to noise propagation to the far field. Hybrid methods can be used instead to tackle this problem according to which the CAA method is used in the near field and the far field is computed by surface integral methods, for example, Kirchhoff (Lyrintzis 2003) and Ffowcs Williams–Hawkings (Crighton *et al.* 1992), which do not require the discretization of the volume field.

Finite element method (FEM) and boundary element method (BEM) have also been applied to duct acoustic problems. Modelling convention of sound by uniform mean flow in a duct is less expensive using BEMs (e.g. Dunn, Tweed & Farassat 1996), as they only require meshing of the body boundary surface. For non-uniform mean flows, FEMs (Eversman & Roy 1993) and the Green's function discretization (GFD) method (Casalino, di Francescantonio & Druon 2004) are also suitable; however, GFD method and FEM require meshing of the entire fluid volume.

In the present work, a BEM formulation is presented, which is an extension of the formulation proposed by Morino (1993) and Gennaretti & Morino (1992) to the frequency domain for scattering problems in conjunction with a spinning rotor source model. Specifically, the method is based on the boundary integral equation (BIE) initially introduced for incompressible aerodynamic problems (Morino, Chen & Suciu 1975) and later on extended to compressible aerodynamic flows (Gennaretti & Morino 1992; Morino 1993) and aeroacoustics (Gennaretti, Luceri & Morino 1997). It has the advantage to be applicable to complex three-dimensional geometries and have the integral coefficient matrices, arising when replacing the BIE with a linear system of algebraic equations, independent of the incident frequency field. Therefore, it is very appealing for multiple frequency computations. Furthermore, Gennaretti & Morino (1992) have developed an extension of the formulation for a frame of reference in rigid motion with respect to the undisturbed air. This formulation can form the basis for predicting the sound convected by a mean swirling flow in a duct, by adding the swirl to the translation of the mean flow. This possibility is explored here with respect to duct aeroacoustics.

The paper is organized as follows. In § 2 the BEM formulation for a helicoidal flow written in the frequency domain is summarized. Investigation of the swirling flow effects on noise radiation to the far field are investigated in § 3 for a generic duct geometry. Finally, § 4 summarizes the conclusions from the present study.

2. Theoretical and computational model

The BEM formulation (Gennaretti & Morino 1992) has been employed for the case of a stationary duct with mean flow convecting an incident acoustic field due to a rotor tonal source of frequency ω. The flow moves in a helicoidal motion with uniform translating velocity $\boldsymbol{v}_\infty$ directed along the duct axis x, and uniform angular velocity Ω_∞, swirling around x. The transformation between the frame of reference $(\boldsymbol{x}, t)$, rigidly connected with the duct, and the frame of reference $(\boldsymbol{\xi}, \tau)$, taken with reference to the undisturbed air, is $\check{\boldsymbol{\xi}}(\boldsymbol{x}, t) = \boldsymbol{U}_\infty(t)\boldsymbol{x} - \boldsymbol{v}_\infty t$, where $\boldsymbol{U}_\infty(t)$ is the rigid-body rotation matrix

$$\boldsymbol{U}_\infty(t) = \begin{bmatrix} 1 & 0 & 0 \\ 0 & \cos \Omega_\infty t & \sin \Omega_\infty t \\ 0 & -\sin \Omega_\infty t & \cos \Omega_\infty t \end{bmatrix}. \tag{2.1}$$

The standard linear wave equation for inviscid flow (without heat conduction) is employed in an integral form in the time domain. The Green's function is written as $G(\boldsymbol{x}, \boldsymbol{x}_\star, t, t_\star) = -1/(4\pi\check{\varrho})\delta(t - t_\star + \theta)$, where δ is the Dirac's function, θ is the time required for a signal to propagate from the source point $\boldsymbol{x}$ to the emission point $\boldsymbol{x}_\star$ and $\check{\varrho}$ is the distance between the two points increased by the convecting factor $(1 + M_r)$ with M_r being the flow Mach number vector projected along the distance vector. For acoustic scattering, the acoustic velocity potential ϕ is represented by $\phi = \hat{\phi}\, \mathrm{e}^{\mathrm{i}\omega t}$ and the formulation is written in a frequency domain as

$$E(\boldsymbol{x}_\star)\hat{\phi}(\boldsymbol{x}_\star) = \int_{S_B} \mathrm{e}^{-\mathrm{i}\omega\theta} \left(\frac{-1}{4\pi\check{\varrho}} \frac{\partial\hat{\phi}}{\partial\tilde{n}} - \frac{\partial}{\partial\tilde{n}} \left(\frac{-1}{4\pi\check{\varrho}} \right) \hat{\phi} + \mathrm{i}\omega\hat{\phi} \frac{-1}{4\pi\check{\varrho}} \left(\frac{\partial\theta}{\partial\tilde{n}} + 2\frac{\boldsymbol{M}\cdot\boldsymbol{n}}{c} \right) \right) \mathrm{d}S, \tag{2.2}$$

where $\partial/\partial\tilde{n} = (\boldsymbol{n} - \boldsymbol{M}\cdot\boldsymbol{n}\ \boldsymbol{M})\cdot\nabla$, with $\boldsymbol{n}$ being the (outwards) vector normal to the body surface S_B; $\boldsymbol{M} = -\boldsymbol{M}_\infty + (\boldsymbol{\Omega}_\infty\boldsymbol{x})/c$ is the Mach vector, for $\boldsymbol{M}_\infty = \boldsymbol{v}_\infty/c$, and $\boldsymbol{\Omega}_\infty$ is the antisymmetric rotation matrix around the axis x. Following Morino & Tseng (1990), the variables of (2.2) are given by

$$\check{\varrho} = |g(\theta)| \quad \text{for} \quad g(\theta) = \left(1 - M_\infty^2\right)c\ \theta + \frac{1}{c}\ \boldsymbol{x}\cdot(\boldsymbol{\Omega}_\infty\boldsymbol{U}_\infty(\theta)\boldsymbol{x}_\star) - \boldsymbol{M}_\infty\cdot\boldsymbol{R}, \tag{2.3}$$

where θ is the unique positive root of the equation for a subsonic flow

$$\left(1 - M_\infty^2\right)\theta^2 + \frac{2}{c^2}\ \boldsymbol{x}\cdot((\boldsymbol{U}_\infty(\theta) - \boldsymbol{I})\boldsymbol{x}_\star) - \frac{2}{c}\ \boldsymbol{R}\cdot\boldsymbol{M}_\infty\theta - \frac{R^2}{c^2} = 0, \tag{2.4}$$

and $\boldsymbol{R}$ is defined as $\boldsymbol{R} = \boldsymbol{x} - \boldsymbol{x}_\star$. The quantity E depends on the position of $\boldsymbol{x}_\star$. If $\boldsymbol{x}_\star$ is in the external field, $E = 1$, or inside the surface S_B, $E = 0$. Equation (2.2) is a boundary integral representation (BIR) for ϕ. If $\boldsymbol{x}_\star$ tends to S_B, then $E = 1/2$ and (2.2) yields a BIE with respect to ϕ.

By expanding the terms of (2.2); decomposing $\nabla\hat{\phi} = \partial\hat{\phi}/\partial n\ \boldsymbol{n} + \nabla_{S_B}\hat{\phi}$, where $\nabla_{S_B}\hat{\phi}$ is the gradient over the body surface S_B; and defining $M_n = \boldsymbol{M}\cdot\boldsymbol{n}$, (2.2) becomes

$$\begin{aligned} E(\boldsymbol{x}_\star)\hat{\phi}(\boldsymbol{x}_\star) = {} & \int_{S_B} \frac{-1}{4\pi\check{\varrho}} \left(1 - M_n^2\right) \frac{\partial\hat{\phi}}{\partial n} \mathrm{e}^{-\mathrm{i}\omega\theta}\, \mathrm{d}S - \int_{S_B} \frac{-1}{4\pi\check{\varrho}} M_n \boldsymbol{M}\cdot\nabla_{S_B}\hat{\phi}\ \mathrm{e}^{-\mathrm{i}\omega\theta}\, \mathrm{d}S \\ & + \int_{S_B} \nabla\left(\frac{-1}{4\pi\check{\varrho}} \right) \cdot (M_n\boldsymbol{M} - \boldsymbol{n})\hat{\phi}\ \mathrm{e}^{-\mathrm{i}\omega\theta}\, \mathrm{d}S \\ & + \mathrm{i}\omega \left[\int_{S_B} \frac{-1}{4\pi\check{\varrho}} \nabla\theta\cdot(\boldsymbol{n} - M_n\boldsymbol{M})\hat{\phi}\ \mathrm{e}^{-\mathrm{i}\omega\theta}\, \mathrm{d}S + 2\int_{S_B} \frac{-1}{4\pi\check{\varrho}} \frac{M_n}{c}\hat{\phi}\ \mathrm{e}^{-\mathrm{i}\omega\theta}\, \mathrm{d}S \right]. \end{aligned} \tag{2.5}$$

In order to evaluate the integral terms, the gradients of the source term $-1/(4\pi\check{\varrho})$, i.e. the doublet term and the delay θ have to be defined. The gradients of $\check{\varrho}$ and θ are obtained by (2.3) and (2.4), respectively,

$$\nabla\check{\varrho} = \begin{cases} \left(\left(1 - M_\infty^2\right)c + \boldsymbol{x}\cdot(\boldsymbol{\Omega}_\infty\boldsymbol{U}'_\infty(\theta)\boldsymbol{x}_\star)/c\right)\nabla\theta + \boldsymbol{\Omega}_\infty\boldsymbol{U}_\infty(\theta)\boldsymbol{x}_\star/c - \boldsymbol{M}_\infty & g(\theta) \geqslant 0, \\ -\left(\left(1 - M_\infty^2\right)c + \boldsymbol{x}\cdot(\boldsymbol{\Omega}_\infty\boldsymbol{U}'_\infty(\theta)\boldsymbol{x}_\star)/c\right)\nabla\theta - \boldsymbol{\Omega}_\infty\boldsymbol{U}_\infty(\theta)\boldsymbol{x}_\star/c + \boldsymbol{M}_\infty & g(\theta) < 0, \end{cases}$$

and $\nabla\theta = (c\boldsymbol{M}_\infty\theta + \boldsymbol{R} - (\boldsymbol{U}_\infty(\theta) - \boldsymbol{I})\boldsymbol{x}_\star)/(c\check{\varrho})$, with $\boldsymbol{U}'_\infty$ being the derivative of $\boldsymbol{U}_\infty$ with respect to θ.

In linear acoustics, the solution is given by adding to the incident field ϕ^I the scattered field, ϕ^S: $\hat{\phi} = \phi^I + \phi^S$. Because the incident field identically satisfies the BIE, (2.5) translates in the frequency domain in terms of the scattered velocity potential and the boundary condition at the body surface is written as $\partial\phi^S/\partial n = -\partial\phi^I/\partial n$.

This formulation consists a suitable model for a wide range of scattering problems in the presence of flow. In fact, for a complex geometry equation (2.5) is written for each part of the body in the appropriate frame of reference, where the flow is modelled as a translation plus a rotation, and the solution is then obtained by a linear superposition.

The numerical implementation of the BIE (2.5) is based on a collocation method. The surface S_B is discretized in N quadrilateral panels and the variables ϕ^S, $\partial\phi^I/\partial n$, M_n and $e^{-i\omega\theta}$ are assumed to be constant on each element surface (zeroth-order method). The integral equation is replaced with a $N \times N$ linear system of algebraic equations with frequency independent integral coefficient matrices.

As an incident field a spinning dipole ring source model has been employed. Following Garrick & Watkins (1953), the rotor load, distributed along a ring of fixed radius r_s and spinning along the azimuth ψ_s, was modelled as a dipole directed along the duct axis x (thrust component) and evaluated by the derivative of the Green's function in (2.2). At the point $\boldsymbol{x}$ (x, r, ψ) for each azimuthal component m of the spinning source, the incident velocity potential is written as

$$\phi^I = \int_0^{2\pi} \frac{1}{4\pi\breve{\varrho}} \left(\frac{1}{\breve{\varrho}} \frac{\partial \breve{\varrho}}{\partial x_s} + i\omega \frac{\partial \theta}{\partial x_s} \right) e^{-i(\omega\theta + m\psi_s)} \, d\psi_s, \tag{2.6}$$

where $\breve{\varrho}$ is defined by

$$\breve{\varrho} = \left| \left(1 - M_\infty^2\right) c \; \theta + \frac{1}{c} \; \boldsymbol{x_s} \cdot (\boldsymbol{\Omega}_\infty \boldsymbol{U}_\infty(\theta)\boldsymbol{x}) - \boldsymbol{M}_\infty \cdot \boldsymbol{R} \right|, \tag{2.7}$$

with θ being the unique positive root of the equation

$$\left(1 - M_\infty^2\right)\theta^2 + \frac{2}{c^2} \; \boldsymbol{x_s} \cdot ((\boldsymbol{U}_\infty(\theta) - \boldsymbol{I})\boldsymbol{x}) - \frac{2}{c} \; \boldsymbol{R} \cdot \boldsymbol{M}_\infty \theta - \frac{R^2}{c^2} = 0, \tag{2.8}$$

for $\boldsymbol{R} = \boldsymbol{x_s} - \boldsymbol{x}$. Therefore, the derivatives are evaluated using (2.7) and (2.8), as

$$\frac{\partial \theta}{\partial x_s} = \frac{c M_{\infty_x} \theta + (x_s - x)}{\breve{\varrho} c}, \tag{2.9a}$$

$$\frac{\partial \breve{\varrho}}{\partial x_s} = \begin{cases} \left(\left(1 - M_\infty^2\right) c + 1/c \; \boldsymbol{x_s} \cdot (\boldsymbol{\Omega}_\infty \boldsymbol{U}'_\infty(\theta)\boldsymbol{x}) \right) \partial\theta/\partial x_s - M_{\infty_x} & \text{if} \quad g(\theta) \geqslant 0, \\ -\left(\left(1 - M_\infty^2\right) c + 1/c \; \boldsymbol{x_s} \cdot (\boldsymbol{\Omega}_\infty \boldsymbol{U}'_\infty(\theta)\boldsymbol{x}) \right) \partial\theta/\partial x_s + M_{\infty_x} & \text{if} \quad g(\theta) < 0, \end{cases} \tag{2.9b}$$

where M_{∞_x} is the component of $\boldsymbol{M}_\infty$ in the axial direction.

Introducing the variable $\psi_1 = \psi_s - \psi$ and the azimuthal mode decomposition $\phi^I(x, r, \psi) = \sum_m \phi_m^I(x, r) e^{-im\psi}$, the spinning modes ϕ_m^I are written as

$$\phi_m^I = \int_0^{2\pi} \frac{1}{4\pi\breve{\varrho}} \left(\frac{1}{\breve{\varrho}} \frac{\partial \breve{\varrho}}{\partial x_s} + i\omega \frac{\partial \theta}{\partial x_s} \right) e^{-i(\omega\theta + m\psi_1)} \, d\psi_1. \tag{2.10}$$

3. Results

3.1. *Comparison with the exact solution*

The computational model was validated against the exact solution of a dipole point source: $\phi = \partial(e^{-i\omega\theta}/(4\pi\breve{\varrho}))/\partial x_s$ (quantities defined as in (2.6)). The velocity potential due to the dipole was compared with the BEM velocity potential scattered from a cylinder when the same dipole providing the boundary condition for the incident field. The cylinder's axis was placed in the x direction and its centre at the coordinate centre.

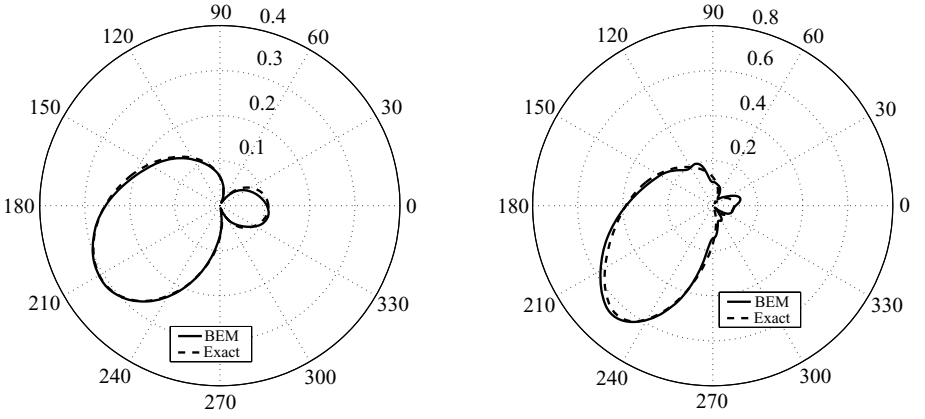

(*a*) $M_\infty = 0.4,\ \Omega_\infty = 0.6$ (*b*) $M_\infty = 0.6,\ \Omega_\infty = 0.6$

FIGURE 1. Comparison of the directivity patterns of the velocity potential generated by a dipole ($ka = 4$) and the BEM solution scattered from a cylinder.

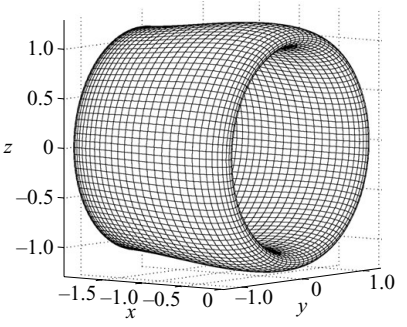

FIGURE 2. Duct geometry.

The cylinder radius a was used as the reference length; the length of the cylinder is $2a$. The dipole, directed along the x-axis, was placed on the z-axis at a distance 0.5 from the origin of the coordinates. The directivity patterns were evaluated on a circle of radius 2 on the x–y plane. Figure 1 shows the results for a dipole source oscillating at the non-dimensional frequency $ka = 4$. The case concerns the superposition of a flow translating along the x-axis and a rotational flow swirling around the same axis. The swirling mean flow angular velocity Ω_∞ was made non-dimensional using a/c as the time scale. The exact and computed velocity potentials agree very well, especially for $M_\infty = 0.4$, while for $M_\infty = 0.6$ some distortion in the directivity pattern is noted. The latter is probably due to the effect of the approximation of the surface gradient integral coefficient, which is more effective for high Mach numbers.

3.2. *Spinning rotor source results*

The computational model was used to investigate the characteristics of the radiation patterns generated by the rotor ring incident field and convected by a swirling-translating mean flow. Figure 2 shows a discretized version of the duct geometry, which was generated by a complete rotation of a Joukowsky profile. The rotor ring of radius 0.9 is placed at one quarter of the duct length, where the duct radius is equal to the reference length scale a. The duct maximum radius at the exhaust is equal to

1.125 and the duct length is 2. The frame of reference is centred at the duct inlet disk as shown in figure 2. The pressure values of the scattered fields were evaluated over a circle of radius D. In order to compare the directivity patterns, the absolute pressure values were normalized with respect to their maximum value. As a measure of the total power radiated from the duct, the power level Π (dB) was also examined:

$$\Pi = 10 \log \left[\frac{\pi D^2/(\rho_\infty c) \int_0^{2\pi} |p|^2 \sin\alpha \, \mathrm{d}\alpha}{P_{ref}} \right]. \tag{3.1}$$

Here $|p|$ is the absolute pressure value calculated using the Bernoulli theorem, ρ_∞ is the reference density and α is a dummy variable. The integral was taken over a circle of radius D and P_{ref} is the reference pressure (10^{-12} W).

In order to simulate a stationary nacelle embedded in still air with a mean flow passing through, the directivity pattern in the far field for a stationary observer was obtained as follows: (i) for the duct in a swirling-translating mean flow the BIE (2.5) was used to calculate the scattered velocity potential on a fictitious cylinder surrounding the duct; (ii) then, for the propagation outside the duct the BIR formulation in the absence of flow was used to calculate the scattered pressure propagating from the fictitious cylinder to the far field. The cylinder radius and length were chosen as 1.4 and 3, respectively, so that the fictitious surface was very close to the duct surface. Numerical investigations using different cylinder lengths and radii showed that these parameters have negligible effects on the results.

The investigation was carried out for different spinning source blade tip Mach numbers M_t from 0.8 to 1.4, and azimuthal orders m from 4 to 12. Furthermore, a negative value of m was also considered in order to investigate the effect of opposite rotation of the spinning source. The resulting non-dimensional frequencies ka were evaluated as $ka = M_t m$. The Mach numbers and rotation velocities of the mean flow (in the x direction) were chosen as $M_\infty = 0.2$, 0.4, 0.6 and $\Omega_\infty = 0$, 0.2, 0.4, 0.6.

The present method has been implemented into parallel computers using the Message Passing Interface (MPI) and the Scalable Linear Algebra PACKage (ScaLAPACK). The computational cost depends directly on the frequency with more panels being required for shorter wavelengths. Grid convergence tests showed that 8000 panels were sufficient at the highest frequency. Using eight nodes of a computer cluster (IBM eServer326 m, dual-core, 2.2G Hz, 1 Gb RAM per core), the computation of a 8000×8000 integral coefficient matrix requires approximately 2 h, while the solver requires 3 min. The allocated memory per node is 64 Mb. Numerical tests showed that increasing the inversion matrix by a factor of 3.5 results in a fivefold increase of the computing time. A lower frequency requires a smaller inversion matrix, thereby reducing the overall computational cost by the above factors.

3.2.1. *Translating flow effect: varying mean flow Mach number*

In order to show the translating flow effect, the directivity pattern of the normalized scattered pressure and the scattered power levels, calculated at a distance $D = 8$, were plotted by varying M_∞ and keeping constant Ω_∞. Figure 3 shows the directivity patterns for the azimuthal order $m = 12$ and angular velocities $\Omega_\infty = 0$, 0.4. The upper and lower sides of the directivity patterns are referred to the different Mach numbers, $M_\infty = 0$, 0.2, 0.4, 0.6. Figure 4 shows the variation of the scattered power level versus the translating flow M_∞ for constant M_t and m.

The effect of the mean flow is clearly remarkable. As predicted by the modal analysis (Goldstein 1976), the modal content increases when the flow Mach number increases.

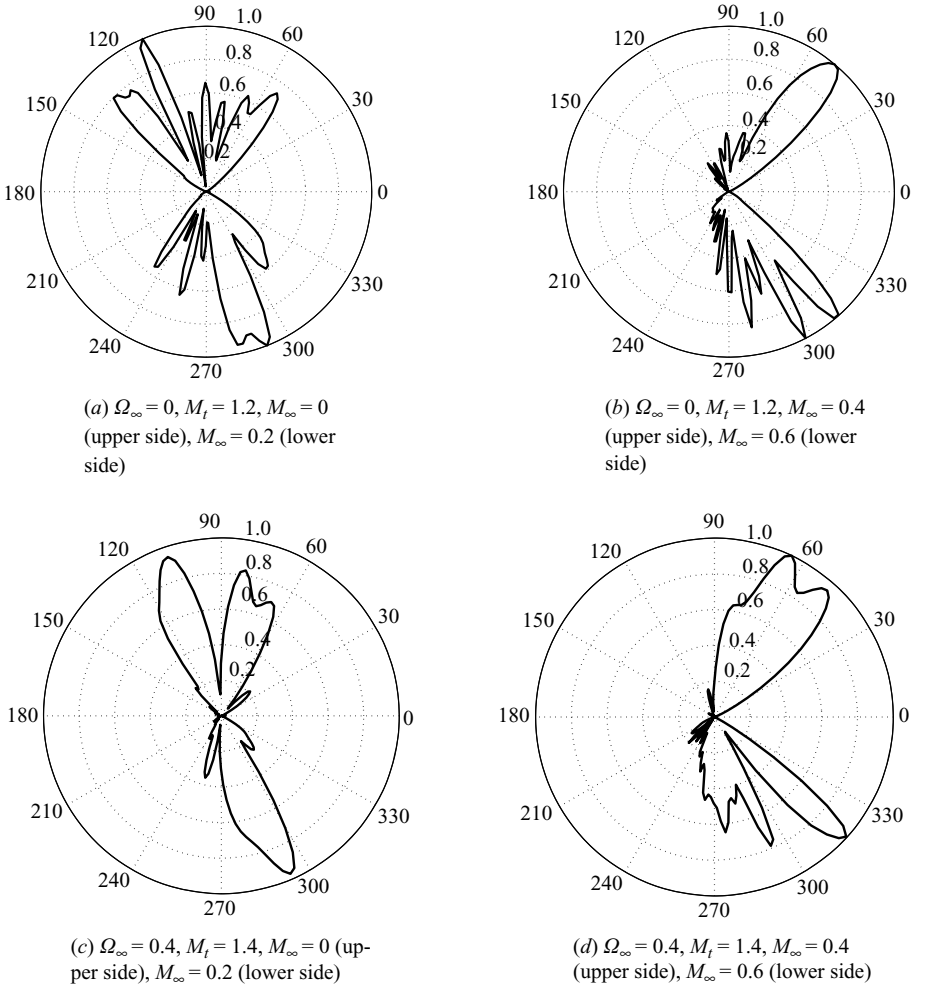

(*a*) $\Omega_\infty = 0$, $M_t = 1.2$, $M_\infty = 0$ (upper side), $M_\infty = 0.2$ (lower side)

(*b*) $\Omega_\infty = 0$, $M_t = 1.2$, $M_\infty = 0.4$ (upper side), $M_\infty = 0.6$ (lower side)

(*c*) $\Omega_\infty = 0.4$, $M_t = 1.4$, $M_\infty = 0$ (upper side), $M_\infty = 0.2$ (lower side)

(*d*) $\Omega_\infty = 0.4$, $M_t = 1.4$, $M_\infty = 0.4$ (upper side), $M_\infty = 0.6$ (lower side)

FIGURE 3. Directivity pattern of the normalized scattered pressure for varying M_∞; $m = 12$.

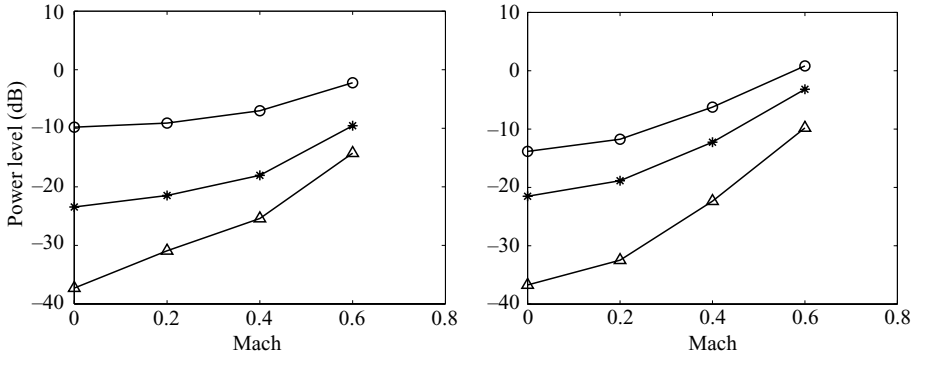

(*a*) $M_t = 1.0$, $\Omega_\infty = 0.4$

(*b*) $M_t = 1.2$, $\Omega_\infty = 0.4$

FIGURE 4. Variation of the scattered power level versus M_∞, for constant m: lines —○— $m = 4$, — * — $m = 8$, —△— $m = 12$. The difference is calculated with respect to the case where there is no mean flow.

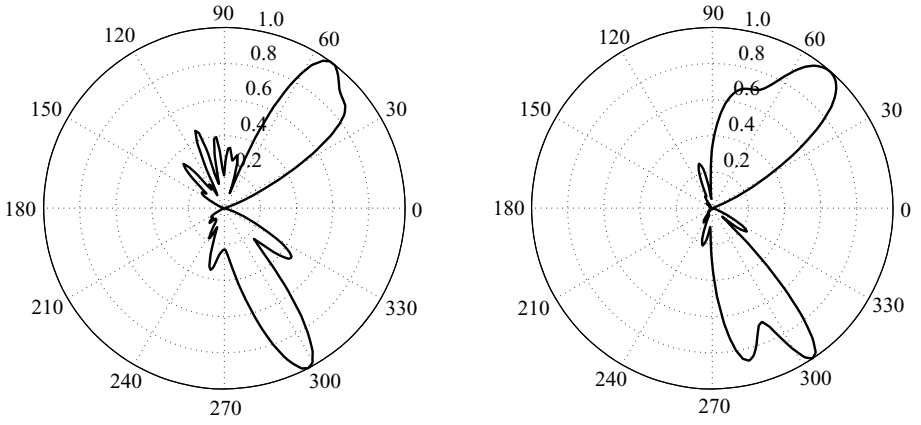

(a) $M_\infty = 0.4$, $M_t = 1.4$, $\Omega_\infty = 0$ (upper side), $\Omega_\infty = 0.2$ (lower side)

(b) $M_\infty = 0.4$, $M_t = 1.4$, $\Omega_\infty = 0.4$ (upper side), $\Omega_\infty = 0.6$ (lower side)

(c) $M_\infty = 0.6$, $M_t = 1.4$, $\Omega_\infty = 0$ (upper side), $\Omega_\infty = 0.2$ (lower side)

(d) $M_\infty = 0.6$, $M_t = 1.4$, $\Omega_\infty = 0.4$ (upper side), $\Omega_\infty = 0.6$ (lower side)

FIGURE 5. Directivity pattern of the normalized scattered pressure with varying Ω_∞; $m = 8$.

In fact, the directivity pattern gets richer in peaks, i.e. more lobes correspond to more cut-on modes (Chapman 1994), and the scattered power level increases. Furthermore, the main lobes of the directivity patterns tend to move downstream.

3.2.2. *Swirling flow effect: varying mean flow angular velocity*

The swirling flow effect was investigated using the directivity pattern of the normalized scattered pressure and the scattered power levels; Ω_∞ was varied for constant M_∞. Figures 5 and 6 show the directivity patterns for the azimuthal orders $m = 8, -8$ and translating flow Mach numbers $M_\infty = 0.4, 0.6$. The upper and lower sides of the directivity patterns are referred to different $\Omega_\infty = 0, 0.2, 0.4, 0.6$. Figure 7 shows the variation of the scattered power level versus the swirling flow angular velocity for constant M_t and m.

The swirling flow does have an effect on the directivity pattern, which is different depending on the case. Both the number and position of the lobes vary. In some cases the downstream lobe is completely shifted. This can be noted for the cases of $M_\infty = 0.6$, $m = 8$, and $M_\infty = 0.4$, $m = -8$ ($\Omega_\infty = 0.6$). In general, as predicted analytically

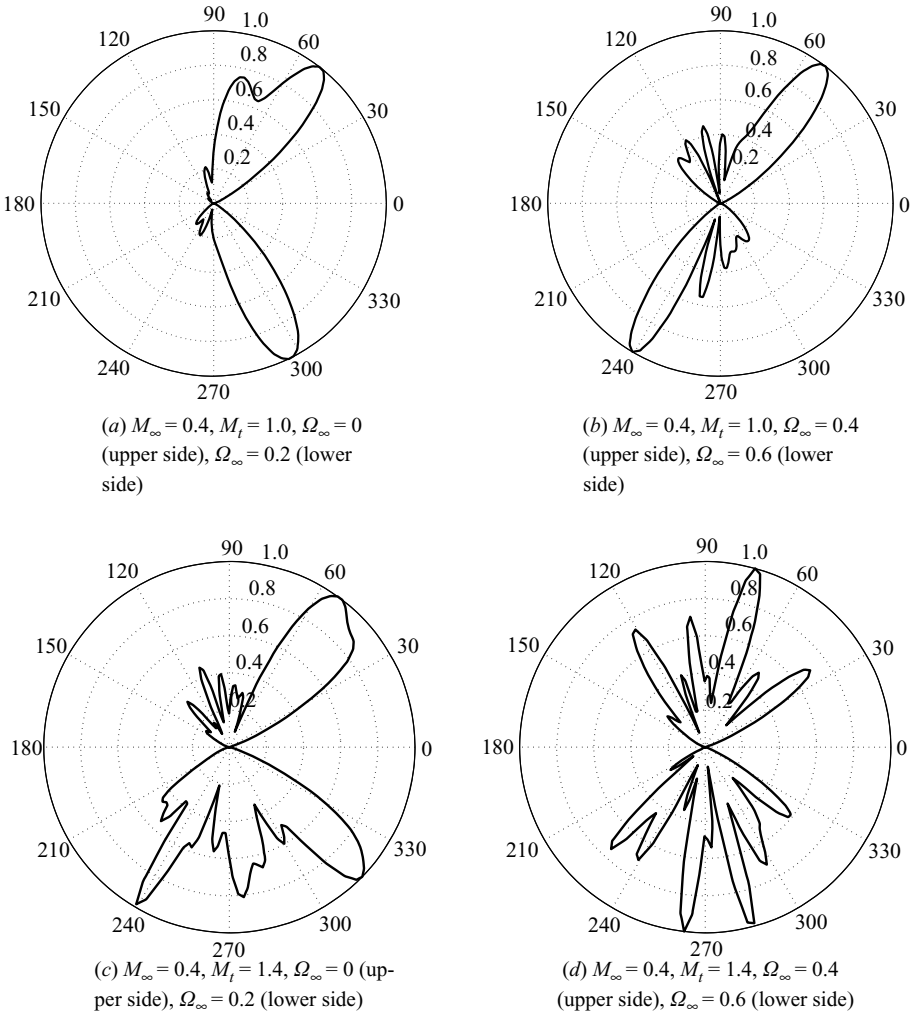

(*a*) $M_\infty = 0.4$, $M_t = 1.0$, $\Omega_\infty = 0$ (upper side), $\Omega_\infty = 0.2$ (lower side)

(*b*) $M_\infty = 0.4$, $M_t = 1.0$, $\Omega_\infty = 0.4$ (upper side), $\Omega_\infty = 0.6$ (lower side)

(*c*) $M_\infty = 0.4$, $M_t = 1.4$, $\Omega_\infty = 0$ (upper side), $\Omega_\infty = 0.2$ (lower side)

(*d*) $M_\infty = 0.4$, $M_t = 1.4$, $\Omega_\infty = 0.4$ (upper side), $\Omega_\infty = 0.6$ (lower side)

FIGURE 6. Directivity pattern of the normalized scattered pressure with varying Ω_∞; $m = -8$.

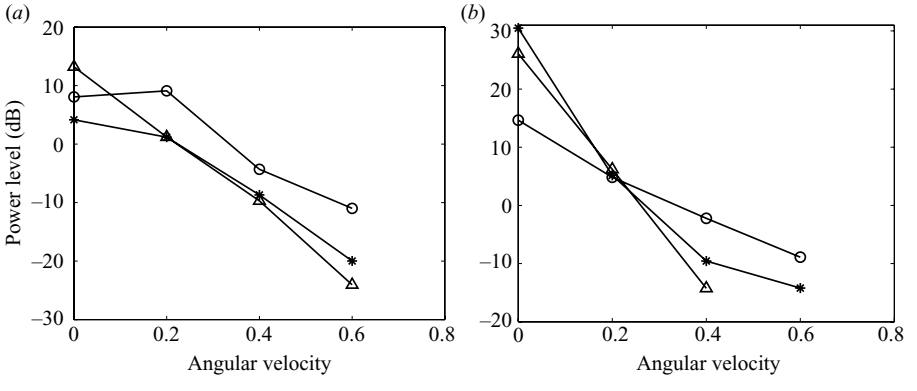

FIGURE 7. Variation of the scattered power level versus Ω_∞. lines $-\circ-$ $m = 4$, $-*-$ $m = 8$, $-\triangle-$ $m = 12$. The difference is calculated with respect to the case where there is no mean flow.

(Cooper & Peake 2005), the swirling flow decreases the modal content when co-rotating with the spinning azimuthal order of the incident source, i.e. fewer lobes correspond to fewer cut-on modes (Chapman 1994). For positive m, the trend of the scattered power level is overall decreasing with Ω_∞, while for negative m the effect is the opposite and less evident. On the other hand, the scattered pressure directivity pattern becomes wider with increasing Ω_∞.

4. Conclusions

The focus of the present investigation was the modelling of the effects of the translating-swirling flow on the noise radiation to the far field using a BEM in the frequency domain. It is well known that the convection of sound is strongly modified by the mean fluid flow. In particular, modes cut on in the absence of mean flow can be cut off in the presence of a swirling flow co-rotating with the spinning azimuthal order, and vice versa. Both the translating flow Mach number and the swirling flow angular velocity affect the directivity pattern of the scattered pressure and the scattered power level. The modal analysis showed that the modal content of the scattered field increases when increasing the translating flow Mach number. This is clearly shown in the variations of the scattered pressure directivity patterns and scattered power levels.

A swirling flow, co-rotating with the azimuthal order of the spinning source, leads to a reduction of the mode propagation. This is confirmed by the trends of the scattered power level, which are decreasing with the mean flow angular velocity. For negative azimuthal order (counter-rotating with respect to the swirl), the scattered pressure directivity patterns show that the lobes increase and the patterns become more complex. However, the effect on the scattered power level is less evident. The mean translating flow seems to move the main lobes of the directivity patterns downstream, whereas in some cases the mean swirling flow appears to neglect this effect and the downstream lobe is completely shifted. This phenomenon will be investigated in a future work with reference to the near field results.

REFERENCES

Casalino, D., di Francescantonio, P. & Druon, Y. 2004 Gfd prediction of fan noise propagation. In *10th AIAA/CEAS Aeroacoustics Conference*, Manchester, UK, *AIAA Paper* 2004–2989.

Chapman, C. J. 1994 Sound radiation from a cylindrical duct. Part I. Ray structure of the duct modes and of the external field. *J. Fluid Mech.* **281**, 293–311.

Cooper, A. J. & Peake, N. 2005 Upstream-radiated rotor-stator interaction noise in a mean swirling flow. *J. Fluid Mech.* **523**, 219–250.

Crighton, D. G., Dowling, A. P., Ffowcs Williams, J. E., Heckl, M. A. & Leppington, F. G. 1992 *Modern Methods in Analytical Acoustics*. Springer.

Dunn, M. H., Tweed, J. & Farassat, F. 1996 The prediction of ducted fan engine noise via a boundary integral equation method. In *2nd AIAA/CEAS Aeroacoustics Conference*, State College, PA, *AIAA Paper* 96–1770.

Eversman, W. & Roy, I. D. 1993 Ducted fan acoustic radiation including the effects of non-uniform mean flow and acoustic treatment. In *15th AIAA/CEAS Aeroacoustics Conference*, Long Beach, CA, *AIAA Paper* 93–4424.

Garrick, I. E. & Watkins, C. W. 1953 A theoretical study of the effect of forward speed on the free-space sound-pressure field around propellers. *Tech. Rep.* TN 3018. NACA.

Gennaretti, M., Luceri, L. & Morino, L. 1997 A unified boundary integral methodology for aerodynamics and aeroacoustics of rotors. *J. Sound Vib.* **200** (4), 467–489.

Gennaretti, M. & Morino, L. 1992 A boundary element method for the potential, compressible aerodynamics of bodies in abitrary motion. *Aeronaut. J.* **96**, 15–19.

Gobulev, V. V. & Atassi, H. M. 2000 Unsteady swirling flows in annular cascades. Part 1. Evolution of incident disturbances. *AIAA J.* **38** (7), 1142–1149.

Goldstein, M. E. 1976 *Aeroacoustics*. McGraw-Hill.

Heaton, C. J. & Peake, N. 2006 Algebraic and exponential instability of inviscid swirling flow. *J. Fluid Mech.* **565**, 279–318.

Lyrintzis, A. S. 2003 Surface integral methods in computational aeroacoustics – from the (cfd) near-field to the (acoustic) far-field. *Intl J. Aeroacoust.* **2** (2), 95–128.

Morino, L. 1993 Boundary integral equations in aerodynamics. *Appl. Mech. Rev.* **46** (8), 445–466.

Morino, L., Chen, L. & Suciu, E. 1975 Steady and oscillatory subsonic and supersonic aerodynamics around complex configurations. *AIAA J.* **13** (3), 368–374.

Morino, L. & Tseng, K. 1990 *Boundary Element Methods in Nonlinear Fluid Dynamics*. Elsevier Applied Science.

Tam, C. K. W. 2006 Recent advances in computational aeroacoustics. *Fluid Dyn. Res.* **38** (9), 591–615.

Tam, C. K. W. & Auriault, L. 1998 The wave modes in ducted swirling flows. *J. Fluid Mech.* **371**, 1–20.